Organic Electronics 17 (2015) 364–370

Contents lists available at ScienceDirect

Organic Electronics

journal homepage: www.elsevier.com/locate/orgel

Performance enhancement in inverted polymer solar cells incorporating ultrathin Au and LiF modified ZnO electron transporting interlayer

Zhe Lu [a], Xiaohong Chen [a,*], Jianping Zhou [b], Ziyao Jiang [a], Sumei Huang [a], Furong Zhu [c], Xianqing Piao [a], Zhuo Sun [a]

[a] Engineering Research Center for Nanophotonics and Advanced Instrument, Ministry of Education, Department of Physics, East China Normal University, Shanghai 200062, China
[b] School of Power and Automation Engineering, Shanghai University of Electric Power, Shanghai 2000902, China
[c] Department of Physics, Centre for Advanced Luminescence Materials, Research Centre of Excellence for Organic Electronics, Hong Kong Baptist University, 224 Waterloo Road, Kowloon Tong, Hong Kong

ARTICLE INFO

Article history:
Received 11 September 2014
Received in revised form 12 December 2014
Accepted 26 December 2014
Available online 3 January 2015

Keywords:
Inverted polymer solar cells
Plasmon resonance
Au nanostructures
Lifetime

ABSTRACT

The performance enhancement of inverted polymer solar cells (PSCs), based on the blend system of regioregular poly(3-hexylthiophene) and [6,6]-phenyl C_{61}-butyric acid methylester, due to incorporating ultrathin Au and LiF interlayer between the front transparent indium tin oxide and a ZnO electron transporting layer was analyzed. The results reveal that a 40% increase in PCE, e.g., from 2.62% to 3.67%, was observed for PSCs made with an optimal Au/LiF interlayer as compared to the one having a bare ZnO electron transporting layer. The presence of Au/LiF-modified ZnO interlayer between ITO and the organic layer helps to improve the charge collection. The absorption enhancement arising from the plasmon resonance of Au nanostructures also contributed to the improvement in PCE. It is shown that PSCs with LiF incorporated ZnO electron transporting layer allow improving cell lifetime, demonstrating <50% decrease in PCE compared to that of the ones with a bare ZnO interlayer after 240 day aging test for cells without encapsulation in air.

1. Introduction

Considerable effort has been devoted to the development of polymer solar cells (PSCs) as a promising alternative photovoltaic technology. Bulk heterojunction PSCs based on low band-gap conjugated polymer and phenyl-C_{70}-butyric acid methylester with power conversion efficiency (PCE) of ~10% were reported [1,2]. However, the PCE of PSCs is still limited by its relatively low carrier mobility. The absorption in PSCs is limited due to a mismatch between light absorption depth and carrier transport scale [3]. Several light trapping techniques, such as diffraction grating, tandem structures and incorporating metal nanostructures, have been developed to increase the optical absorption of solar cells [4].

The absorption enhancement in PSCs incorporating metal nanostructures has been demonstrated due to its enhanced near-field and forward light scattering caused by the nanostructures [4–6]. In previous reports, metal nanostructures are usually incorporated into the buffer and photoactive layer, inserted between tandem cells, and attached onto the electrodes [4,5,7–10]. The plasmonic enhancement of PSCs is partially contributed by the incorporation of metal nanostructures [7,10,11]. Meanwhile, our reports have shown the deteriorating performance of

* Corresponding author. Tel.: +86 21 62233676.
E-mail address: xhchen@phy.ecnu.edu.cn (X. Chen).

http://dx.doi.org/10.1016/j.orgel.2014.12.032
1566-1199/

PSCs made with metal nanostructures due to a higher serial resistance and lower shunt resistance. This increases interfacial barrier at organic/electrode interfaces, metal nanoparticle-induced carrier traps and carrier combinations [12]. The improved electrical conductivity of buffer layer and photoactive layer is considered as an important factor for enhancing PCE in PSCs [8,9,13]. Kim et al. reported 50–70% improvement in PCE of PSCs, which is primarily attributed to the improved electrical conductivity of the photoactive layer doped with Au and Ag nanoparticles [8]. Theoretical simulations showed that the incorporation of metal nanostructures in PSCs can greatly increase the optical absorption of photoactive layers [5,6]. Optimal carrier collecting/transporting layers are used to inhibit defects in photoactive layers penetrated into the whole PSCs [14], which are very important for the application of PSCs with nanoparticles. Solution-processed ZnO nanoparticles are commonly used as a good electron transport/collecting layer in inverted PSCs [15,16] due to their relatively high transparency, high electron mobility and air stability. Recently, fullerene derivative [17], conjugated polyelectrolytes [18], poly(ethylene oxide) [19], ionic liquid functionalized carbon nanoparticles [20,21] and cesium stearate [22] have been reported to modify ZnO layer to optimize contact properties between ZnO, photoactive layer and passivate traps of bulk ZnO layer, improving the photocurrent and fill factor of PSCs. In a related work, we found that the dissociation of excitons at the electrode/organic interface in PSCs plays an important role in determining the charge collection in regular and inverted PSCs. The unfavorable exciton dissociation at the organic/electrode interface for charge collection can be eliminated by interposing a thin metal oxide interlayer between the organic layer and electrode [23]. In this work, the presence of a dual interlayer consisting of ultrathin Au and LiF layers between ITO and ZnO is able to improve the contact quality of ZnO layer for application in inverted PSCs. The enhancement in PCE of PSCs with ZnO layer, modified with Au/LiF and LiF layers, is observed compared to that of control PSCs made with bare ZnO layer. In addition to the absorption enhancement due to plasmonic effect, the improvement in the contact quality at ZnO/ITO interface also results in cells with a lower serial resistance, which is contributed by the Au/LiF bilayer leading to a significant enhancement in the performance of PSCs.

2. Experimental

Bulk heterojunction PSCs, based on poly(3-hexylthiophene) (P3HT) and [6,6]-phenyl C_{61} butyric acid methyl ester (PCBM) blend system, were fabricated. The pre-patterned ITO/glass substrates, having a sheet resistance of 10 Ω/□, were cleaned by ultrasonication sequentially with detergent, de-ionized water, acetone and isopropanol for 15 min. After being dried in the oven, ITO glass substrates were treated with ultraviolet ozone for 15 min before spin-coated with a layer of ZnO, Au and LiF layers were thermally deposited on ZnO under the base pressure of 6.0×10^{-4} Pa. A ~20 nm thick ZnO electron transport/collecting layer was spin-coated on top of ITO/glass or Au/LiF-modified ITO/glass substrates, followed by annealing at 140 °C for 10 min in air. The ZnO nanoparticles were prepared as described in the previous paper [24,25]. The typical synthesis, a stoichiometric amount of tetramethylammonium hydroxide dissolved in ethanol (0.5 M) was gradually dropped into 0.1 M zinc acetate dihydrate dissolved in dimethyl sulfoxide (DMSO), followed by stirring for an hour at room temperature. After being washed with hexane and ethanol (2:1) mixing solvents, ZnO nanoparticles were dispersed in ethanol. Solutions containing P3HT:PCBM (10 mg/ml:8 mg/ml) dissolved in 1,2-dichlorobenzene were spin-coated on top of a layer of ZnO to form a 60 nm ultrathin photoactive layer in Ar-purged glove box, and then kept in a petri dish for slow growth. After 2 h, P3HT:PCBM films were annealed at 120 °C for 10 min. Finally, a 10 nm thick MoO_3 and 100 nm Al electrode were thermally evaporated onto P3HT:PCBM films in the chamber with the base pressure of 6.0×10^{-4} Pa to form an anode. The active area of the devices is 0.10 cm^2. Current density–voltage (J–V) characteristics were measured under AM1.5G illumination intensity of 100 mW/cm^2 using a Newport solar simulator system. All samples were measured in air without encapsulation. The work function of modified ITO films was measured using ultraviolet photoelectron spectroscopy (UPS) with He-I line (21.2 eV).

3. Results and discussion

The thin layer of Au, deposited by thermal evaporation on ITO surface, is easily aggregated forming Au islands due to the dewetting effect, and further formed into larger islands after annealing [26,27]. SEM images measured for Au films and ZnO films on ITO surface are shown in Fig. 1(a)–(d). It is clear that Au nanoparticles formed after a 0.9 nm thick Au layer was annealed at 140 °C. The size of Au nanoparticles onto ITO coated glass is 10–15 nm. Although the Au granules, overlapped with ZnO, cannot be observed directly in the SEM images, the size of Au granules formed on the ITO surface is expected to be larger than 15 nm due to the Au metal agglomerations which can be partially blocked by the ZnO films in the SEM measurements [27]. The contrast of SEM images measured for Au/LiF modified ZnO films increases substantially as compared to that obtained for LiF/ZnO films. The lighter areas mean higher electrical conductivity [7], indicating the existence of Au islands under ZnO films. The presence of the ZnO layer also helps to avoid the exciton recombination on the Au islands from the photoactive layer [13].

The absorption spectra of ZnO and Au/LiF modified ZnO films are shown in Fig. 1(e). The absorption spectrum of the LiF-modified ZnO film is similar to that of the ZnO film, indicating that a thin LiF film cannot affect the optical properties of ZnO electron transport layers. The absorption of Au/LiF modified ZnO films increases significantly as compared to the bare ZnO films. The protruding absorption at 530 nm of Au/LiF modified ZnO film indicates that the evaporated Au film overlapped with ZnO film were further agglomerated larger islands after annealing 140 °C for 10 min. Fig. 1(e) shows the absorption spectra of P3HT:PCBM formed on different ZnO layers. The absorption

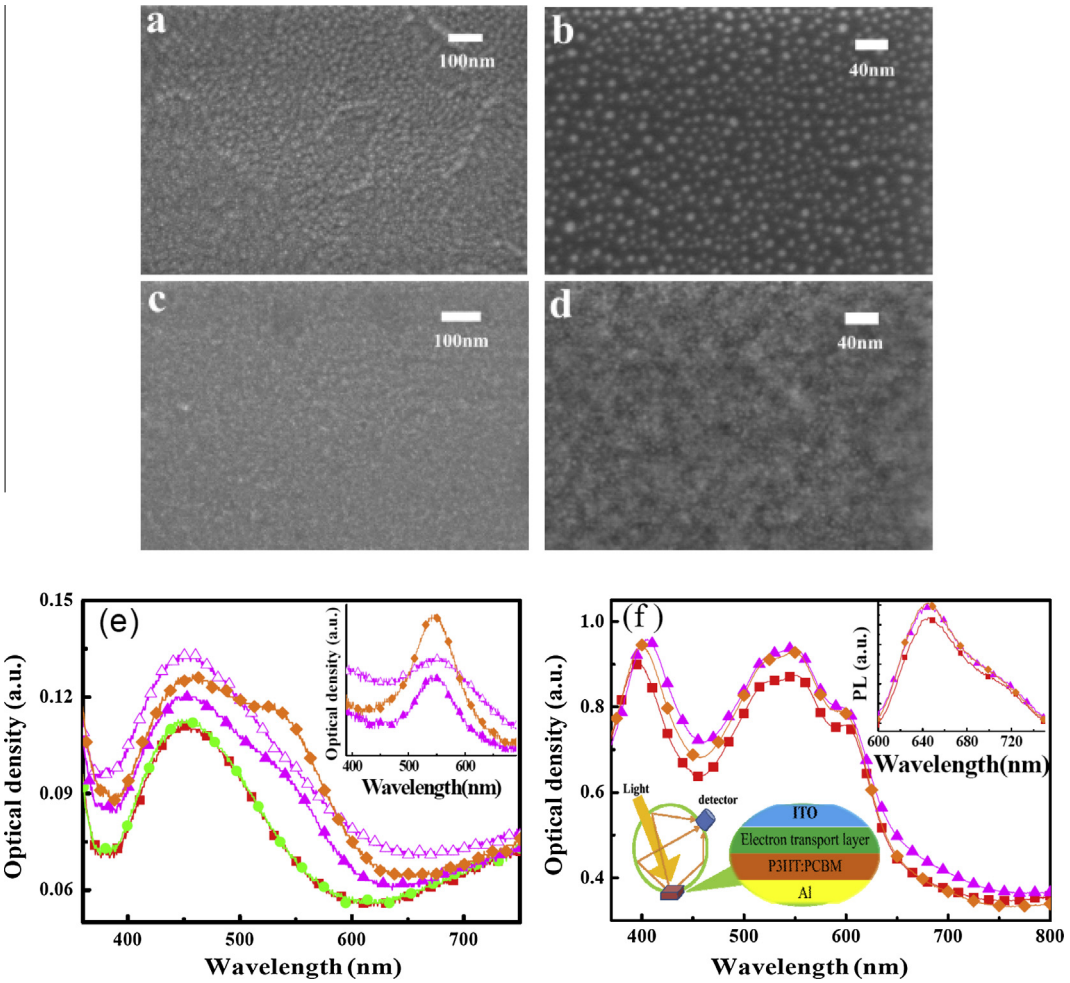

Fig. 1. SEM images measured for different films of Au(0.9 nm) evaporated onto (a) ITO coated glass and (b) silicon after annealing at 140 °C, (c) ZnO and (d) Au(0.9 nm)/LiF(1.0 nm)/ZnO annealing at 140 °C for 10 min. (e) Absorption spectra of ITO/electron transport layers consisting of Au(0.6 nm)/ZnO (△) without annealing, and ZnO(■), LiF(1.0 nm)/ZnO(●), Au(0.6 nm)/LiF(1.0 nm)/ZnO(▲) and Au(0.9 nm)/LiF(1.0 nm)/ZnO(♦) annealing at 140 °C for 10 min, and further subtracted absorption of ITO/ZnO films to obtain absorption spectra (inset) of Au(0.6 nm) (△), annealing Au(0.6 nm) (▲) and Au(0.9 nm) (♦) films. (e) Absorption and PL (inset) spectra of ITO/electron transport layer/P3HT:PCBM/Al with various electron transport layers of ZnO (■), Au(0.6 nm)/LiF(1.0 nm)/ZnO(▲), Au(0.9 nm)/LiF(1.0 nm)/ZnO(♦). Without MoO_3 layer reducing optical interference. The numbers denote average layer thickness in nanometer in all figures.

of P3HT:PCBM layers formed on Au/LiF modified ZnO layers increased significantly as compared to that of the same blend layer on the bare ZnO layer. The improvement in absorption cannot be simply interpreted as enhanced absorption in the photoactive layer of P3HT:PCBM, because the absorption of Au granules cannot be completely excluded. The plasmon resonance wavelength is related to the size and shape of Au granules and the permittivity of the surrounding dielectric [11,13]. The broad absorption of Au agglomerations over the whole visible light range is different from the absorption of those small sized Au nanoparticles formed by the chemical synthesis [28]. The enhanced absorption in P3HT:PCBM layer, induced due to the plasmonic effect of Au agglomerations, are consistent with previous reports [10,13]. The enhanced PL spectra of P3HT:PCBM film with Au/LiF modified ZnO layers, as shown in the inset in Fig. 1(e), further suggest that the plasmon effects of Au islands contribute to P3HT:PCBM photoactive layer [28].

To investigate the effect of LiF and Au incorporated into ZnO electron transport layer on the PCE of PSCs, a set of eleven different types of PSCs were made for comparison studies. The cross-sectional view of a typical PSC with a structure of ITO/Au(*X*)/LiF(*Y*)/ZnO/P3HT:PCBM/MoO_3/Al is shown in the inset of Fig. 2. *X* and *Y* in the parentheses stand for the thickness of Au and LiF layers. Fig. 2 shows the *J*–*V* characteristics measured for the best device of five types. The average values of the cell parameters and their standard deviations measured for the PSCs fabricated with different nominal thickness of the Au layer are summarized in Table 1. The J_{sc}, FF, V_{oc} and PCE of PSCs with LiF modified ZnO layer show improvements compared to that made with only ZnO layer, suggesting that incorporating the LiF layer can greatly reduce contact barrier of ITO/

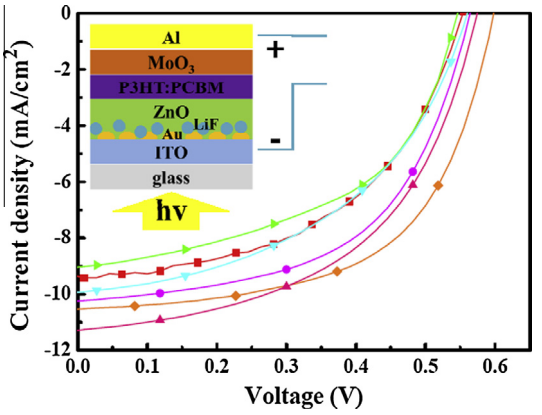

Fig. 2. Current density–voltage characteristics of the best PSC representing each distinct structure. Electron transport layer is ZnO(■), LiF(1.0 nm)/ZnO(●), Au(0.6 nm)/ZnO(▼), Au(0.9 nm)/ZnO(►), Au(0.6 nm)/LiF(1.0 nm)/ZnO(▲), Au(0.9 nm)/LiF(1.0 nm)/ZnO(♦). The inset is a schematic of device structure.

ZnO interface, which is supported by the lower series resistance R_s of 10.33 Ω. The R_s of PSCs is defined by the inverse slope of J–V at J_{sc} = 0 mA/cm^2 under illumination. As for Au/ZnO electron transport layer, the performance of PSC decreases slightly as compared to PSC with a bare ZnO electron-transporting layer. However, the performance of PSCs improved substantially after the Au(0.9 nm)/LiF(1.0 nm) bilayer was incorporated into ZnO electron transport layer. 40% improvement in the PCE of best PSC with Au/LiF modified ZnO layer is observed, with an increase in PCE from 2.62% to 3.67%, which is comparable to PCE of PSCs with conventional photoactive layer thickness of 80–200 nm [27]. However, the average PCE of PSCs decreased from 3.50% to 2.51% when Au layer thickness increased from 0.9 nm to 1.5 nm. The increased R_s of PSCs with Au(1.5 nm)/LiF(1.0 nm) possibly result in an important factor of deteriorated J_{sc}, FF and PCE, indicating that the performance of PSCs is closely related to the serial resistance of PSCs.

To clearly demonstrate the influence of the serial resistance on the performance of PSCs, the parameters of PSCs with Au layer modified by LiF with different thicknesses are listed in Table 2. After 0.9 nm Au film is modified with 1.0–3.0 nm thick LiF layer, J_{sc}, V_{oc}, FF and PCE of PSCs show great improvements compared to PSCs with only Au film. By increasing the thickness of LiF, LiF layers serve as insulators that result in lower J_{sc}, PCE and higher R_s [11]. The difference of near-field enhancement between metal islands and photoactive layers can reasonably be omitted in the range of several nanometers LiF thickness [29]. Therefore, the deteriorated PCE of PSCs with Au(0.9 nm)/LiF(3.0–5.0 nm) compared to Au(0.9 nm)/LiF(1.0 nm) is attributed to higher R_s and higher contact resistance at ITO/ZnO interface as the thickness of the LiF layer increases. Conversely, the average R_s of PSCs with Au(0.9 nm)/LiF(1.0 nm) is only 9.01 Ω, which is obviously lower R_s of 10.33 Ω of PSCs with LiF(1.0)/ZnO layers, indicating that increasing PCE of PSCs with Au(0.9 nm)/LiF(1.0 nm) compared to PSCs with LiF(1.0 nm)/ZnO layer is at least in part attributed to their lower serial resistance.

The incident photon-to-electron conversion efficiency (IPCE) characteristics of five types of PSCs are shown in Fig. 3(a). The wavelength range of spectral response of PSCs with LiF and Au/LiF modified ZnO layers are enhanced compared to PSCs with only ZnO and Au modified ZnO layers. The IPCE measured for PSCs made with Au/LiF modified ZnO interlayer has an obvious enhancement over the whole visible light wavelength range, suggesting Au/LiF modified ZnO also favors the charge collection as manifested in the decrease in the contact resistance. The change in the shape of IPCE spectra measured for PSC with Au/LiF modified ZnO interlayer due to the plasmonic effect of the Au agglomerations also contribute to the improved photocurrent in PSCs [7,11]. Fig. 3(b) shows the normalized IPCE curves to that of PSCs with only the ZnO layer. The relative curve of PSC with LiF modified ZnO is almost flat in the wavelength range from 470 nm to 660 nm. However, the relative curves of PSCs incorporated with Au film shows a dip in the wavelength range from 620 nm to 660 nm, which are irrelative with J_{sc} values. These relative curves roughly match the extinction spectrum profiles of the Au islands, indicating the plasmon resonance effects of Au islands are associated with the photocurrent of PSCs incorporated with Au films [11]. The lacking obvious improvement J_{sc} of PSCs with Au(0.9 nm)/LiF(1.0 nm)/ZnO compared to LiF/ZnO layer is possibly attributed to the absorption and back scattering effect of Au islands, which in part offsets the enhanced absorption of photoactive layer from the near-field enhancement and forward scattering effects of Au nanostructures [5,29].

The serial resistance of PSCs is primarily from bulk resistance of P3HT:PCBM, ZnO electron transport layer and MoO_3 layer, electrodes and contact resistance between different layers. For a PSC with ZnO electron transport layer system, the reduced R_s of PSCs is probably from lower bulk resistance of ZnO layer and lower contact barrier at ITO/ZnO interface [14]. Fig. 4 shows various work function of modified ITO electrode with UPS spectra. The LiF evaporated onto ITO leads to a reduction of work function of ITO,

Table 1
Average cell parameters and the standard deviations measured for PSCs with different Au layer thicknesses.

Au(nm)/LiF(nm)	V_{oc} (V)	J_{sc} (mA/cm^2)	FF	PCE (%)	R_s (Ω cm^2)	R_{sh} (Ω cm^2)
0/0	0.55 ± 0.01	9.42 ± 0.40	0.50 ± 0.01	2.51 ± 0.11	13.00 ± 1.0	417.22 ± 40
0/1	0.56 ± 0.01	10.44 ± 0.22	0.53 ± 0.02	3.18 ± 0.07	10.33 ± 1.0	465.13 ± 60
0.6/1	0.57 ± 0.01	11.28 ± 0.20	0.51 ± 0.01	3.23 ± 0.11	11.53 ± 1.0	429.43 ± 20
0.9/1	0.59 ± 0.01	10.51 ± 0.31	0.57 ± 0.01	3.50 ± 0.18	9.01 ± 0.5	677.10 ± 50
1.2/1	0.58 ± 0.01	10.73 ± 0.26	0.53 ± 0.01	3.30 ± 0.12	10.32 ± 0.6	537.92 ± 20
1.5/1	0.57 ± 0.01	9.42 ± 0.40	0.51 ± 0.01	2.51 ± 0.20	13.46 ± 2.0	450.14 ± 20

Table 2
Average cell parameters and the standard deviation obtained for PSCs with Au layer modified by LiF having different thicknesses.

Au(nm)/LiF(nm)	V_{oc} (V)	J_{sc} (mA/cm^2)	FF	PCE (%)	R_s (Ω cm^2)	R_{sh} (Ω cm^2)
0.6/0	0.56 ± 0.01	9.47 ± 0.57	0.46 ± 0.01	2.50 ± 0.17	14.45 ± 0.8	414.75 ± 20
0.9/0	0.56 ± 0.01	8.21 ± 0.10	0.53 ± 0.01	2.45 ± 0.07	15.0 ± 1.0	339.96 ± 30
0.9/1	0.59 ± 0.01	10.51 ± 0.31	0.57 ± 0.01	3.50 ± 0.18	9.01 ± 0.5	677.10 ± 50
0.9/3	0.60 ± 0.01	10.13 ± 0.10	0.57 ± 0.01	3.37 ± 0.05	9.78 ± 1.0	587.87 ± 20
0.9/4	0.61 ± 0.01	8.55 ± 0.30	0.57 ± 0.01	3.01 ± 0.15	12.49 ± 1.0	793.57 ± 10
0.9/5	0.61 ± 0.01	7.88 ± 0.30	0.54 ± 0.01	2.62 ± 0.20	13.72 ± 1.0	792.54 ± 10

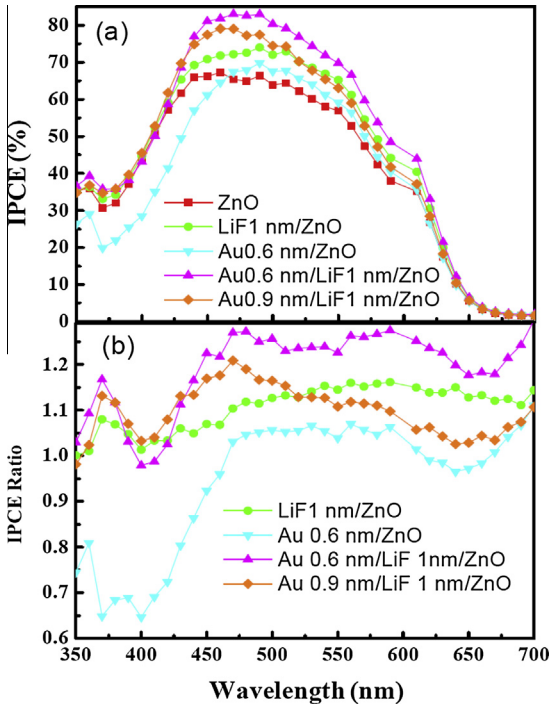

Fig. 3. (a) IPCE characteristics of PSCs with different electron transport layer. (b) IPCE curves normalized to that of PSC with ZnO layer. Curves showing the ratio of IPCE for LiF(1.0 nm)/ZnO(●), Au(0.6 nm)/ZnO(▼), Au(0.6 nm)/LiF(1.0 nm)/ZnO(▲) and Au(0.9 nm)/LiF(1.0 nm)/ZnO(♦) divided by that for ZnO.

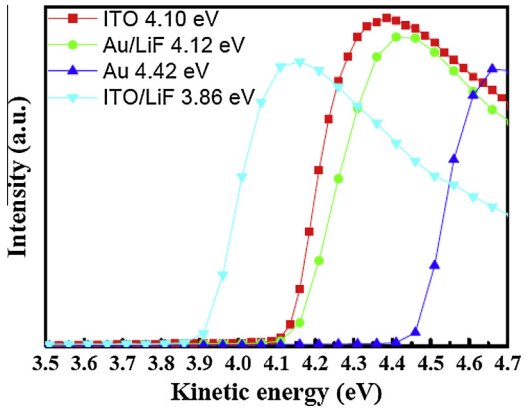

Fig. 4. UPS spectra of thin films for ITO (■), ITO/LiF(●), ITO/Au(0.6 nm)(▼) and ITO/Au(0.6 nm)/LiF(▲).

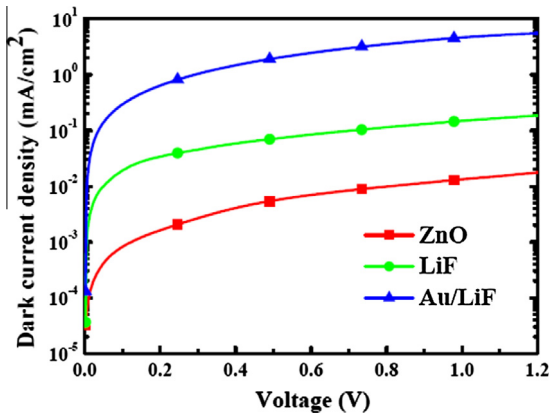

Fig. 5. The dark *J*–*V* characteristic curves of electron-only devices ITO/electron transporting layer/P3HT:PCBM/LiF/Al.

consistent with previous reports for LiF on ITO [30]. The work function of Au modified ITO is reduced from 4.42 eV to 4.12 eV after LiF modified Au film. This supports improved performances of PSCs with Au(0.9 nm)/LiF(1.0 nm) compared to PSCs with only Au film. This is also consistent with the observations on metal surfaces with reduction reported for LiF by UPS [31] and the observations of PSCs with LiF/Al or Au electrodes improved PCE compared to PSCs with only Al or Au electrodes [32]. Fig. 5 shows *J*–*V* characteristics measured for electron-only devices with the configuration of ITO/electron transporting layers/P3HT:PCBM/LiF/Al in the dark condition. The electrons are collected by the front ITO cathode under forward bias, which is similar to electron transporting process in PSCs. The improved current density of electron-only device with Au/LiF and LiF modified ZnO interlayer, compared to the bare ZnO layer, further suggested that Au/LiF and LiF modified ZnO layer can help to improve electron extraction in PSCs. Considering lower work-function (3.86 eV) of ITO/LiF, compared to work function (4.12 eV) of ITO/Au/LiF, the increase in the photocurrent of electron-only device at 1.2 V suggests that the conductivity of Au/LiF modified ZnO interlayer is also improved [8]. Improved electron transport and extraction is an efficient method to decrease carrier combination, thereby V_{oc} of PSCs [10,33]. Compare to the control device with a bare ZnO interlayer, the reduced interface contact barrier and improved conductivity of Au/LiF-modified ZnO interlayer contribute to the enhancement in V_{oc} (0.6 V) and FF of the PSCs with Au/LiF-modified ZnO interlayer, avoiding the defects trap-

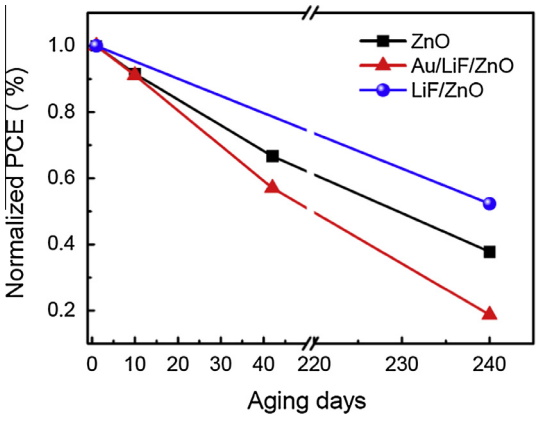

Fig. 6. Normalized PCE of PSCs with aging time. PSCs with ZnO (■), Au/LiF/ZnO(▲) and LiF/ZnO(●).

assisted charge recombination at the cathode/organic interface in PSCs [16].

In addition to the PCE of PSCs, the stability of PSCs is also a key factor for the commercialization of PSCs. The PCE of the conventional PEDOT:PSS based PSCs exhibited a rapid PCE degradation due to acidic property of PEDOT:PSS. Inverted PSCs are preferred as the reverse configuration avoids the use of corrosive PEDOT:PSS hole transporting layer on transparent conducting oxide anode to improve the operation stability [4,16]. Fig. 6 shows the normalized PCE of PSCs as a function of aging time. The PSCs without encapsulation were kept in drying cabinet with a low relativize humidity of <10% under ambient atmosphere. The PCE of PSCs with Au/LiF modified ZnO layer and pure ZnO layer remain at 91% of the initial PCE value after aging 10 days, indicating that Au/LiF modified ZnO layers have a good stability. Especially, the PCE of PSCs with LiF modified ZnO layer still remains more than 50% after aging 240 days, suggesting LiF modified ZnO layer can improve stability of PSCs. As for ITO/LiF system, ITO surface is rich in O^{2-} after UV–ozone treatment, which can absorb Li^{+} ions forming oriented LiF dipole array on ITO surface [34], resulting in lower work function of ITO, as shown in Fig. 4. The existence of LiF dipole layer possibly offsets in part deterioration at ITO/ZnO interface with time pass away. Furthermore, Li (F) diffused into ZnO layer prefers to occupy interstitial sites, which can produce electrons, improve carrier concentration and decrease bulk resistance of ZnO layer [35]. The results of this work agree with our finding in showing that the improvement in the cathode/organic contact quality is a perquisite for a significant enhancement in performance of inverted PSCs [23].

4. Conclusions

In conclusion, inverted PSCs with optimized Au/LiF and LiF modified ZnO electron transporting layer showed 40% and 26% improved PCE over PSCs with a bare ZnO electron transporting layer. The reduced contact barrier and improved conductivity of Au/LiF-modified ZnO interlayer on the surface of the front ITO electrode are primary responsible for improved performance of inverted PSCs. The absorption enhancement in photoactive layer due to plasmonic effect only plays a secondary role to improve PCE of PSCs. The PSCs with LiF modified ZnO layer demonstrate improved air stability as compared to PSCs with a bare ZnO layer. Less than 50% of the drop in PCE for PSCs with LiF modified ZnO (not encapsulated) was observed after 240 days aging test in air.

Acknowledgments

This work was supported by National Natural Science Foundation of China (Grant Nos. 61275038, 11274119 and 51102095), HKBU Strategic Development Fund (SDF13-0531-A02) and Research Fund for the Doctoral Program of Higher Education of China (Grant Nos. 20110076120017 and 20110076120023).

References

[1] J. You, L. Dou, K. Yoshimura, T. Kato, K. Ohya, T. Moriarty, K. Emery, C.-C. Chen, J. Gao, G. Li, A polymer tandem solar cell with 10.6% power conversion efficiency, Nat. Commun. 4 (2013) 1446.
[2] L. Bian, E. Zhu, J. Tang, W. Tang, F. Zhang, Recent progress in the design of narrow bandgap conjugated polymers for high-efficiency organic solar cells, Prog. Polym. Sci. 37 (2012) 1292.
[3] H. Liu, Z. Wu, J. Hu, Q. Song, B. Wu, H.L. Tam, Q. Yang, W.H. Choi, F. Zhu, Efficient and ultraviolet durable inverted organic solar cells based on an aluminum-doped zinc oxide transparent cathode, Appl. Phys. Lett. 103 (2013) 043309.
[4] Q. Gan, F.J. Bartoli, Z.H. Kafafi, Plasmonic-enhanced organic photovoltaics: breaking the 10% efficiency barrier, Adv. Mater. 25 (2013) 2385.
[5] H. Shen, P. Bienstman, B. Maes, Plasmonic absorption enhancement in organic solar cells with thin active layers, J. Appl. Phys. 106 (2009) 073109.
[6] A. Williamson, É. McClean, D. Leipold, D. Zerulla, E. Runge, The design of efficient surface-plasmon-enhanced ultra-thin polymer-based solar cells, Appl. Phys. Lett. 99 (2011) 093307.
[7] F.-C. Chen, J.-L. Wu, C.-L. Lee, Y. Hong, C.-H. Kuo, M.H. Huang, Plasmonic-enhanced polymer photovoltaic devices incorporating solution-processable metal nanoparticles, Appl. Phys. Lett. 95 (2009) 013305.
[8] K. Kim, D.L. Carroll, Roles of Au and Ag nanoparticles in efficiency enhancement of poly (3-octylthiophene)/C 60 bulk heterojunction photovoltaic devices, Appl. Phys. Lett. 87 (2005) 203113.
[9] X. Li, Z. Deng, Y. Yin, L. Zhu, D. Xu, Y. Wang, F. Teng, Efficiency enhancement of polymer solar cells with Ag nanoparticles incorporated into PEDOT:PSS layer, J. Mater. Sci.: Mater. Electron. 25 (2014) 140.
[10] P. Xu, L. Shen, F. Meng, J. Zhang, W. Xie, W. Yu, W. Guo, X. Jia, S. Ruan, The role of Ag nanoparticles in inverted polymer solar cells: surface plasmon resonance and backscattering centers, Appl. Phys. Lett. 102 (2013) 123301.
[11] X. Chen, C. Zhao, L. Rothberg, M.-K. Ng, Plasmon enhancement of bulk heterojunction organic photovoltaic devices by electrode modification, Appl. Phys. Lett. 93 (2008) 123302.
[12] A.Y. Mahmoud, J. Zhang, D. Ma, R. Izquierdo, V.-V. Truong, Thickness dependent enhanced efficiency of polymer solar cells with gold nanorods embedded in the photoactive layer, Sol. Energy Mater. Sol. Cells 116 (2013) 1.
[13] X. Wang, J.W. Ho, Q. Yang, H.L. Tam, G.X. Li, K.W. Cheah, F. Zhu, Performance enhancement in organic photovoltaic devices using plasma-polymerized fluorocarbon-modified Ag nanoparticles, Org. Electron. 12 (2011) 1943.
[14] F. Zhu, X. Chen, J. Zhou, Z. Lu, Y. Chen, S. Huang, Z. Sun, Enhanced efficiency of inverted polymer solar cells using two-step sputtered ZnO as cathode interfacial layer, Mater. Res. Express 1 (2014) 025020.
[15] Z. Kam, Q. Yang, X. Wang, B. Wu, F. Zhu, J. Zhang, J. Wu, Enhanced absorbance and electron collection in inverted organic solar cells:

optical admittance and transient photocurrent analyses, Org. Electron. 15 (2014) 1306.
[16] J. Liu, S. Shao, B. Meng, G. Fang, Z. Xie, L. Wang, X. Li, Enhancement of inverted polymer solar cells with solution-processed ZnO–TiOX composite as cathode buffer layer, Appl. Phys. Lett. 100 (2012) 213906.
[17] Y.-S. Cheng, S.-H. Liao, Y.-L. Li, S.-A. Chen, Physically adsorbed fullerene layer on positively charged sites on zinc oxide cathode affords efficiency enhancement in inverted polymer solar cell, ACS Appl. Mater. Interfaces 5 (2013) 6665.
[18] T. Hu, F. Li, K. Yuan, Y. Chen, Efficiency and air-stability improvement of flexible inverted polymer solar cells using ZnO/poly (ethylene glycol) hybrids as cathode buffer layers, ACS Appl. Mater. Interfaces 5 (2013) 5763.
[19] S. Shao, K. Zheng, T.n. Pullerits, F. Zhang, Enhanced performance of inverted polymer solar cells by using poly (ethylene oxide)-modified ZnO as an electron transport layer, ACS Appl. Mater. Interfaces 5 (2013) 380.
[20] F. Zhu, X. Chen, L. Zhou, J. Zhou, J. Yang, S. Huang, Z. Sun, Dependence of the performance of inverted polymer solar cells on thickness of an electron selective ZnO layer deposited by magnetron sputtering, Thin Solid Films 551 (2014) 131.
[21] F. Zhu, X. Chen, Z. Lu, J. Yang, S. Huang, Z. Sun, Efficiency enhancement of inverted polymer solar cells using ionic liquid-functionalized carbon nanoparticles-modified ZnO as electron selective layer, Nano-Micro Lett. 6 (2014) 24.
[22] G. Wang, T. Jiu, J. Li, P. Li, X. Song, F. Lu, J. Fang, Interface modification of ZnO-based inverted PTB7:PC71BM organic solar cells by cesium stearate and simultaneous enhancement of device parameters, ACS Sust. Chem. Eng. 2 (2014) 1331.
[23] B. Wu, Z. Wu, H.L. Tam, F. Zhu, Contrary interfacial exciton dissociation at metal/organic interface in regular and reverse configuration organic solar cells, Appl. Phys. Lett. 105 (2014) 103302.
[24] W. Cheng, Z. Wu, S. Wen, B. Xu, H. Li, F. Zhu, W. Tian, Donor–acceptor copolymers incorporating polybenzo [1, 2-b: 4, 5-b′] dithiophene and tetrazine for high open circuit voltage polymer solar cells, Org. Electron. 14 (2013) 2124.
[25] L. Qian, J. Yang, R. Zhou, A. Tang, Y. Zheng, T.-K. Tseng, D. Bera, J. Xue, P.H. Holloway, Hybrid polymer–CdSe solar cells with a ZnO nanoparticle buffer layer for improved efficiency and lifetime, J. Mater. Chem. 21 (2011) 3814.
[26] X. Sun, X. Chen, Z. Zhang, Z. Sun, Plasmon based antireflection coatings containing nanostructured Ag and silica medium, Appl. Surf. Sci. 258 (2012) 3785.
[27] L. Zhou, X. Chen, F. Zhu, X. Sun, Z. Sun, Improving temperature-stable AZO–Ag–AZO multilayer transparent electrodes using thin Al layer modification, J. Phys. D: Appl. Phys. 45 (2012) 505103.
[28] M.-F. Xu, X.-Z. Zhu, X.-B. Shi, J. Liang, Y. Jin, Z.-K. Wang, L.-S. Liao, Plasmon resonance enhanced optical absorption in inverted polymer/fullerene solar cells with metal nanoparticle-doped solution-processable TiO2 layer, ACS Appl. Mater. Interfaces 5 (2013) 2935.
[29] S.A. Maier, H.A. Atwater, Plasmonics: localization and guiding of electromagnetic energy in metal/dielectric structures, J. Appl. Phys. 98 (2005) 011101.
[30] H.S. Kim, H. Lee, P.E. Jeon, K. Jeong, J.H. Lee, Y. Yi, Revised hole injection mechanism of a thin LiF layer introduced between pentacene and an indium tin oxide anode, J. Appl. Phys. 108 (2010) 053701.
[31] N. Watkins, Y. Gao, Vacuum level alignment of pentacene on LiF/Au, J. Appl. Phys. 94 (2003) 1289.
[32] C.J. Brabec, S.E. Shaheen, C. Winder, N.S. Sariciftci, P. Denk, Effect of LiF/metal electrodes on the performance of plastic solar cells, Appl. Phys. Lett. 80 (2002) 1288.
[33] K. Vandewal, K. Tvingstedt, A. Gadisa, O. Inganäs, J.V. Manca, On the origin of the open-circuit voltage of polymer–fullerene solar cells, Nat. Mater. 8 (2009) 904.
[34] J. Wang, F. Zhang, L. Li, Q. An, J. Zhang, W. Tang, F. Teng, Enhanced performance of polymer solar cells by dipole-assisted hole extraction, Sol. Energy Mater. Sol. Cells 130 (2014) 15.
[35] J. Chang, Z. Lin, C. Zhu, C. Chi, J. Zhang, J. Wu, Solution-processed LiF-doped ZnO films for high performance low temperature field effect transistors and inverted solar cells, ACS Appl. Mater. Interfaces 5 (2013) 6687.